

- No.978-1-4673-5999-3/13/31.00 Ac 2013 IEEE.
9. Belyaev B. A., Leksikov A. A., Serzhantov A. M., Shabanov V. F. (2008). Controllable Liquid-Crystal Microwave Phase Shifter. *TECHNICAL PHYSICS LETTERS*, Vol. 34 No 6.
 10. Z.M. Huang, D.Y. Zhang, Y.Q. Luo, J.F. Li, C.L. Liu. A new configuration for phase control in laser coherent combination utilizing liquid crystal optical modulator. *Applied physics*, Ac Springer, Verlag 2010.
 11. B. T. P. Madhav, VGKM Pisipati, N. V. K Ramesh, Habibulla Khan, P. V. Datta Prasad, "PLANAR INVERTED-F ANTENNA ON LIQUID CRYSTAL POLYMER SUBSTRATE FOR PCS, UMTS, WIBRO APPLICATIONS," *ARPJ Journal of Engineering and Applied Sciences*, Vol. 6, No 4, APRIL 2011.
 12. F. A. Tahir, H. Aub ert "EQUIVALENT ELECTRICAL CIRCUIT FOR DESIGNING MEMS-CONTROLLED REFLECTARRAY PHASE SHIFTERS" *Progress In Electromagnetics Research*, PIER,100, 1^a^12, 2010.
 13. Zhou Du, Ville Viikari, Juha Ala-Laurinaho, Aleksi Tamminen, Antti V. R. A^ais A anen. Antenna Pattern Retrieval from Reflection Coefficient Measurements with Reflective Loads. *Progress In Electromagnetics Research*, PIER, Vol. 148, 15 a 22, 2014
 14. Z. G. Wang, B. Yan, R. M. Xu, and Y. C. Guo "Design of a KU band six bit phase shifter using periodically loaded-line and switched-line with loaded-line" *Progress In Electromagnetics Research*, PIER,76, 369 a^379, 2007.



Wellbore Temperature Distribution in Hydraulic-Fracturing Horizontal Wells for Gas

Junjun Cai*, Yonggang Duan

State Key Laboratory of Oil and Gas Reservoir Geology and Exploitation, Southwest Petroleum University, Chengdu 610500, Sichuan, P.R. China

Abstract

Use of distributed temperature sensors (DTS) to monitor the productive zones of horizontal wellbores by real-time temperature profile measurement is becoming an industry standard. Well completion method, skin factor and non-Darcy flow phenomenon are among operating parameters potentially related to DTS data. In order to study on the above-mentioned relationship, this paper establishes temperature models which consider skin factor and non-Darcy flow, in turn whose foundation are mass-, momentum-, and energy-balance equations. The models presented here account for heat convection, fluid expansion, heat conduction and viscous dissipative heating. Once configured, these models were applied to predict wellbore temperature distribution and analyze factors influencing the wellbore temperature profile. Arriving temperature and wellbore temperature curves are plotted by

computed iterative calculation. By analyzing the sensitivity of non-Darcy flow factor and skin factor, we conclude that temperature along the wellbore is related to both factors. Temperature response type curves show that the larger the preset skin factor is, the smaller will be the resulting wellbore temperature. In addition, greater non-Darcy flow factor may generate greater decrease in temperature along the wellbore. Thirdly, varying well completion methods show different temperature distributions along the wellbore. These observations indicate that this model provides an alternative perspective for description of downhole physical characteristics in hydraulic fracturing horizontal wells.

Key words: TEMPERATURE MODEL, GAS RESERVOIRS, HYDRAULIC FRACTURING HORIZONTAL WELLS, TEMPERATURE DISTRIBUTION, SENSITIVITY ANALYSIS

1. Introduction

Hydraulic-fracturing horizontal wells have been used widely to enhance extractive production by increasing wellbore access to the target reservoir. Due to well completion methods and other factors, the local inflow rates along a horizontal well may still vary. Recently, advanced technology, such as distributed temperature sensors (DTS), have been installed on horizontal wellbores as a part of well completion, which new technology provides us continuous, accurate downhole temperature data. Thus, it is possible to reveal the downhole physical characteristics from interpretation of measured temperature and pressure data, for which a temperature distribution model for hydraulic-fracturing horizontal wellbores is necessary.

Temperature logs have been used successfully in vertical wells to locate gas entry, detect casing leaks, evaluate cement placement and estimate inflow profiles [1]. Interpretations of temperature profiles in horizontal wells were reported 10 years ago as useful for identifying the types of fluid flowing in a wellbore [2, 3]. In 2004, Foucault et al. [4] used DTS data to detect the water entry location in a horizontal well. Fryer et al. [5] monitored real time temperature profiles to identify and correlate production changes in a multi-zone reservoir well in 2005. Moreover, Johnson et al. [6] and Huebsch et al. [7] calculated gas flow profiles from measured DTS data. Julian et al. [8] showed that DTS data can be used to determine leak locations in vertical wells. Huckabee [9] applied DTS data to diagnose fracture stimulation and evaluate well performance. In 2010, Li et al. [10] observed DTS bottom-level reservoir temperature data, plus inversed inflow profile along the horizontal section and set up a downhole inflow control valve (ICV) to research the relationship between temperature profile and inflow profile. Gonzalez et al. [11] found conventional testing methods unsuitable for the development of shale gas reservoirs, and presented a DTS technology application able to provide continuous, real-time downhole information to describe shale gas well frac-

turing and production.

Temperature models began with temperature logging. Thus far, researchers have put forward some models to simulate temperature changes under both steady-state and varying conditions. In 1962, Ramey [12] posited the earliest temperature model. Based on Ramey's model and considering the condensation factor, that is, the change of phase state, Satter [13] modified the model of steam injection wells to calculate heat loss and wellbore temperature. In 1972, Witterholt et al. [14] proposed a model describing heat exchange between fluid, wellbore and reservoir, by which the wellbore temperature and surrounding reservoir temperature distribution are calculated. The following year, Steffensen R J et al. [15] reported a Joule-Thomson effect generated by pressure loss where fluid flux can significantly affect the temperature curve. Miller [16] presented one of the earliest transient-temperature-of-reservoir models in 1980, which model also predicts how temperature changes in a reservoir will be affected by fluid inflow or outflow from a wellbore. The following decade, Sagar et al. [17] established a general model to predict temperature profiles in two-phase-flow wells, while extending Ramey's equation to inclined wells and accounting for the Joule-Thomson effect caused by pressure change along the wellbore. Subsequently, Hasan and Kabir [18] developed Ramey's model further. Izgec et al. [19] developed a coupled wellbore-reservoir model for transient fluids and heat flow. By analytic methods, Yoshioka et al. [20] studied horizontal wellbore temperature, while Zhuoyi Li [21] also researched horizontal wellbore temperature phenomena using numerical solution.

On the basis of previous works, this paper establishes both wellbore and reservoir models, as well as a coupled model, which consider skin factor and non-Darcy flow. Arriving temperature, which impacts temperature along wellbore, is also investigated here, and wellbore temperature distribution curves of fracturing horizontal wells are plotted. Finally, the effects of relevant parameters and different well completion

methods are also analyzed.

2. Model Development

The overall model consists of a wellbore model, a reservoir model and a coupled model, which models are detailed in the following sections.

2.1 Wellbore Model

For this study, the wellbore model developed by Yoshioka et al. [22] was adopted directly, which consists of both wellbore flow and wellbore thermal models. Wellbore flow and thermal behaviors are treated here as steady-state phenomena.

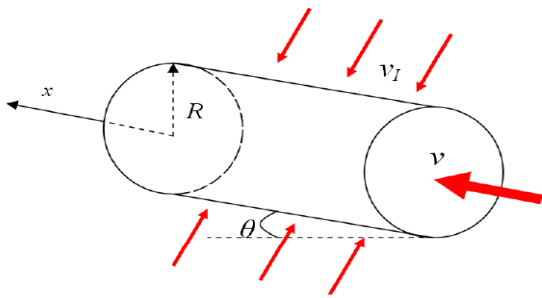


Figure 1. Differential volume element of a wellbore

2.1.1 Wellbore Flow Model

The mass conservation equation for a given well-

$$\frac{dT_{well}}{dx} = K_{IT} \frac{dp_{well}}{dx} + \frac{2(\gamma\rho_1 v_1 C_p + (1-\gamma)U_T)}{R \rho v_x C_p} (T_I - T_{well}) - \frac{g}{C_p} \sin \theta \tag{3}$$

The general expression of γ was first proposed by Willhite [26], where

$$U_{T,I} = \gamma(\rho v C_p)_{T,I} + (1-\gamma)U_T \tag{4}$$

In this case, heat conduction between fluids is also neglected. In terms of this model, therefore, the heat flux in the open pipe area consists of only convection as depicted in Figure 2.

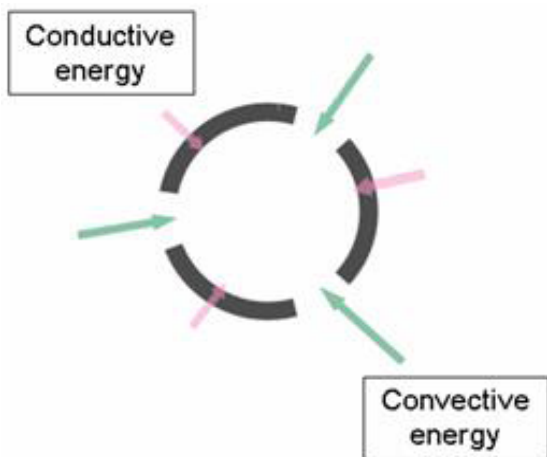


Figure 2. Energy transport through a perforated/slotted pipe

bore under steady-state conditions is:

$$\frac{d(\rho v_x)}{dx} = \frac{2\gamma}{R} \rho_1 v_1 \tag{1}$$

where γ is the ratio of the open section versus the total well length.

According to momentum balance, the pressure equation is obtained by the following formula:

$$\frac{dp_{well}}{dx} = -\frac{\rho f v_x^2}{R} - \frac{d(\rho v_x v_x)}{dx} - \rho g (\sin \theta) \tag{2}$$

Here, f is the friction factor, which was established as a model for horizontal wells by Ouyang[23] in 1998.

2.1.2 Wellbore Thermal Model

Based on the energy balance equation for wellbore temperature, a horizontal well is assumed to be in a steady state, with one-dimensional temperature. Ignoring kinetic shear, viscous shear and heat transfer between fluids, the ultimate one-dimensional, single-phase, steady-state wellbore temperature equation is[27]:

2.2 Reservoir Model

2.2.1 Mass Balance

The mass balance for fluid flow in permeable media is given as:

$$\frac{\partial}{\partial t} (\rho_g S_g \phi) + \nabla \cdot (\rho_g \bar{u}_g) = 0 \tag{5}$$

while, according to Darcy's law, the Darcy velocity is:

$$\bar{u} = -\frac{k}{\mu} \cdot (\nabla p + \rho \bar{g}) \tag{6}$$

In this work, a numerical simulation (Eclipse, 2006) was used solve the above equations.

2.2.2 Energy Balance

Neglecting kinetic energy change and considering convection, conduction, viscous dissipation and thermal expansion in the heat-transfer problem, while also dropping the time derivative term, yields[20]:

$$\rho C_p (\bar{u} \cdot \bar{\nabla} T_R) - \beta T_R (\bar{u} \cdot \bar{\nabla} p_R) - \bar{\nabla} \cdot (K_{T_R} \bar{\nabla} T_R) + \bar{u} \cdot \bar{\nabla} p_R = 0 \tag{7}$$

In this study, no flow in the z-direction within the reservoir is assumed. Here, we use the finite-difference method to find the reservoir's temperature distribution. When not otherwise specified, the top and

bottom boundaries are assigned a constant temperature, while all other reservoir boundaries are set equal

$$AP_{i,j,k} T_{i,j,k}^{n+1} = AW_{i,j,k} T_{i-1,j,k}^{n+1} + AE_{i,j,k} T_{i+1,j,k}^{n+1} + AS_{i,j,k} T_{i,j-1,k}^{n+1} + AN_{i,j,k} T_{i,j+1,k}^{n+1} + B_{i,j,k} \quad (8)$$

In this case, all parameters can be solved by numerical dispersion, from which we obtain the following large linear matrix of temperature equations:

$$\mathbf{A} \mathbf{T} = \mathbf{B} \quad (9)$$

where \mathbf{A} is the coefficients matrix, \mathbf{T} is the unknown temperature vector, and \mathbf{B} is the source term. Coefficients matrix \mathbf{A} has five linear domains, which include non-zero elements, while all other elements in matrix \mathbf{A} are zero. From here, a program can be developed to solve this set of equations to obtain the temperature in a gas reservoir.

2.3 Coupled Model

The objective of the coupled model is to find the arriving temperature, T_l , which is dependant on method of well completion. For a well contained in the grid, Figure 3 illustrates the thermal/flow system used in this work.

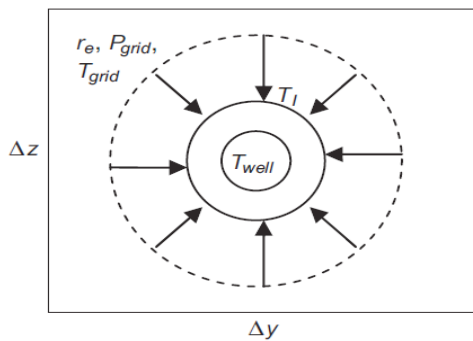


Figure 3. Integrated temperature behavior

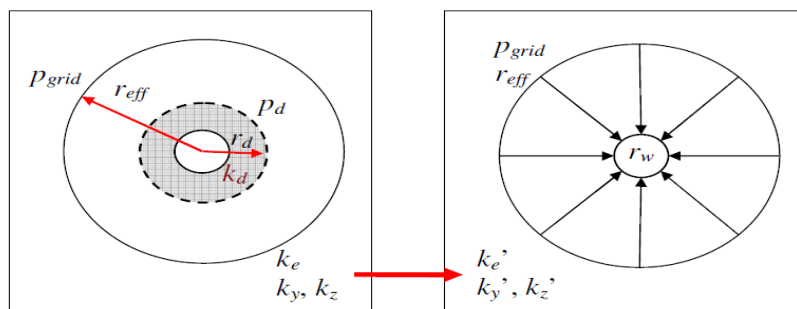


Figure 4. Estimate formation damage effect by effective permeability

In this situation, gas viscosity is low and gas flow velocity is usually very high, especially in the area near the wellbore. Considering non-Darcy flow, the relationship between pressure and flow rate is:

$$\psi_g - \psi_{wf} = aq_{sc} + bq_{sc}^2 \quad (12)$$

where a is the Darcy flow factor and b is the non-Darcy flow factor. Here, ψ represents pseudo-pressure as:

to distributed geothermal temperature. The resulting finite-difference equation is:

2.3.1 Engaged Reservoir and Wellbore

For this investigation, the model of a coupled reservoir and wellbore developed by Zhuoyi Li[21] was adopted directly. The arriving temperature, T_p , as the link between reservoir grid temperature and wellbore temperature, must be found to solve temperature equations 3 and 7. Hence, the pressure from the grid to the wellbore becomes:

$$\frac{d^2 p}{dr^2} + \frac{1}{r} \frac{dp}{dr} = 0 \quad (10)$$

By combining equations 7 and 10 under appropriate boundary conditions, we obtain the arriving temperature thus: $T_l = T|_{r=r_w}$.

During drilling, well completion and/or production, formation damage may occur, increasing loss of pressure and affecting temperature behavior at a given flow rate. Stabilized grid distribution is one approach which prevents formation damage, which damage can now be estimated by use of effective permeability. Assuming that the formation damage is within radial range, as shown in Figure 4, where permeability is represented by k_d and radius by r_d , the effective permeability is derived as:

$$k_e = \ln \frac{r_{eff}}{r_w} \cdot \left(\frac{1}{k_e} \ln \frac{r_{eff}}{r_d} + \frac{1}{k_d} \ln \frac{r_d}{r_w} \right)^{-1} \quad (11)$$

$$\psi = 2 \int_{p_0}^p \frac{p}{\mu z} dp \quad (13)$$

2.3.2 Disengaged Reservoir and Wellbore

When the reservoir and wellbore are not engaged, pressure changes in the reservoir have no effect on the pressure in the wellbore, since there is no fluid interaction between the reservoir and wellbore. In this case, Equation 7 becomes:

$$\frac{1}{r} \frac{d}{dr} \left(r \frac{dT}{dr} \right) = 0 \quad (14)$$

As well, the concomitant boundary conditions would be:

$$T = T_{\text{grid}} \quad r = r_{\text{eff}} \quad (15)$$

and

$$K_{\text{Tt}} \frac{dT}{dr} \Big|_{r=r_w} = U_{\text{T}} \left(T \Big|_{r=r_w} - T_w \right) \quad r = r_w \quad (16)$$

Solving Equation 14, we obtain the arriving temperature, T_I , of no connection between reservoir and wellbore. According to the behavior of these equations, reservoir grid, arriving temperature and wellbore temperature are bound by interaction.

3. Solution Procedure

During solution, the interactive nature of grid and

temperature characteristics is in full play. Solving first for gas reservoir pressure distribution, wellbore pressure is consequently also solved. Next, apply the found reservoir pressure value to solve for reservoir temperature. Finally, solve wellbore temperature using the coupled model iteratively until the solution reaches convergence, which procedure is detailed in Figure 5. Convergence condition is defined by a relative error of less than 10^{-6} , which may be calculated by the equation below.

$$\frac{(\tilde{T}_{\text{well}}^i - \tilde{T}_{\text{well}}^{i+1})^T (\tilde{T}_{\text{well}}^i - \tilde{T}_{\text{well}}^{i+1})}{(\tilde{T}_{\text{well}}^i)^T (\tilde{T}_{\text{well}}^i)} < 10^{-6} \quad (17)$$

where $\tilde{T}_{\text{well}}^i$ is the matrix of wellbore temperature, and superscript T is the transpose of the matrix.

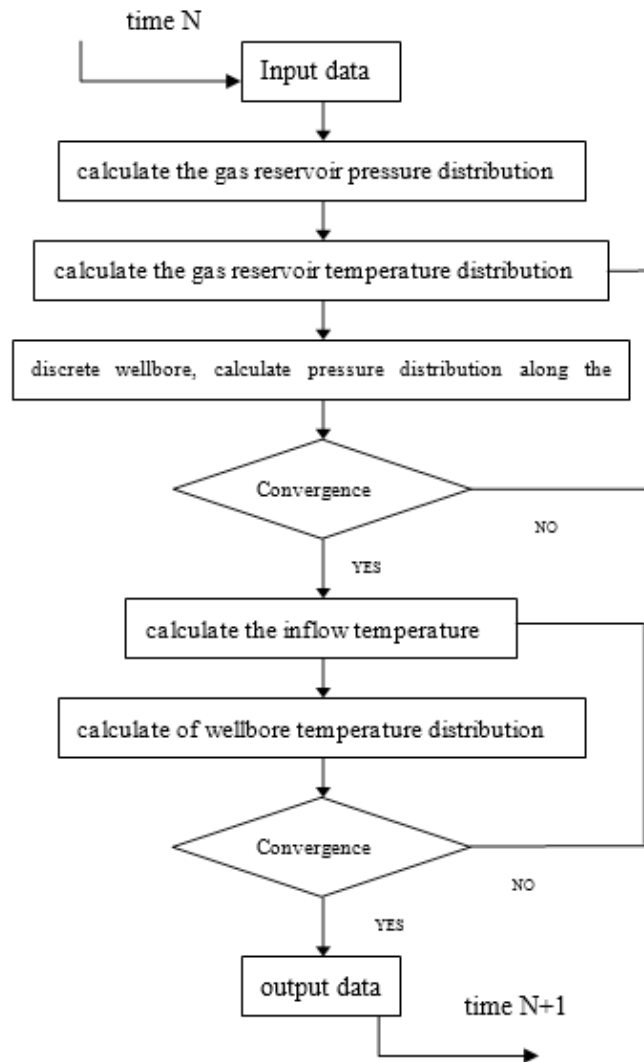


Figure 5. Calculation procedure for temperature distribution along the wellbore

4. Results And Discussions

As shown above, we may obtain the reservoir temperature and wellbore temperature iteratively. The model well considered here is completed, cased and

perforated (Fig. 6); plus, it is assumed that the well is producing at a constant rate of 24000m³/d. The production profile is shown in Figure 7, while details of the well and reservoir properties are shown in **Table 1**.



Figure 6. Synthetic well completion method

Table 1. Basic parameters of reservoir and well

Parameters	value
Reservoir depth (m)	2000
Initial reservoir temperature (Degrees Celsius)	82
Initial reservoir pressure(Mpa)	28.5
Permeability (mD)	10
Reservoir thickness (m)	10
Gas density (kg/m ³)	150
Heat capacity [J/(kg·(Degree Celsius))]	2150
Total heat conductivity [w/m·(degree Celsius)]	2.25
Reservoir size (m×m×m)	600×890×10
Grid size	60×89×1
Horizontal well length (m)	600
Well radius (m)	0.1
ID (m)	0.066
OD (m)	0.0889
Pipe wall: relative roughness	0.01

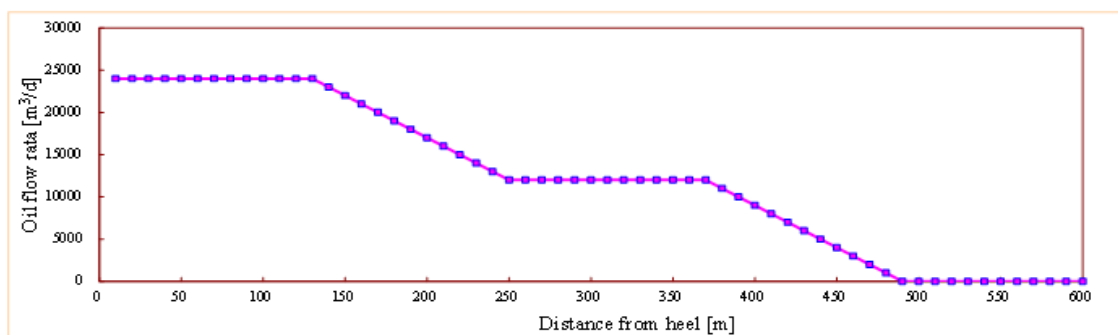


Figure 7. Gas flow rate profile in synthetic example

The arriving temperature, T_l , is related to skin factors and the perforated locations. Figure 8 depicts comparison between the arriving temperature profile comparison with and without the skin factor, wherein arriving temperature in consideration of skin factor is lower than that without skin factor. The cause of this difference is that greater pressure loss is generated near the wellbore under damaged formation condi-

tions, leading to reduced arriving temperature as the result of the Joule-Thomson effect. Another factor of concern is change in arriving temperature along the perforated sections, which holds the line along the non-perforated sections.

Temperature along the wellbore is also related to skin factor and the perforated locations. As shown in Figure 9, a clear influence is effected by skin factor on the wellbore temperature.

Temperature along the non-perforated section changes very little, whereas changes along the perforated sections are obvious. Also revealed in the be-

low figure is increased wellbore temperature with decreasing skin factor.

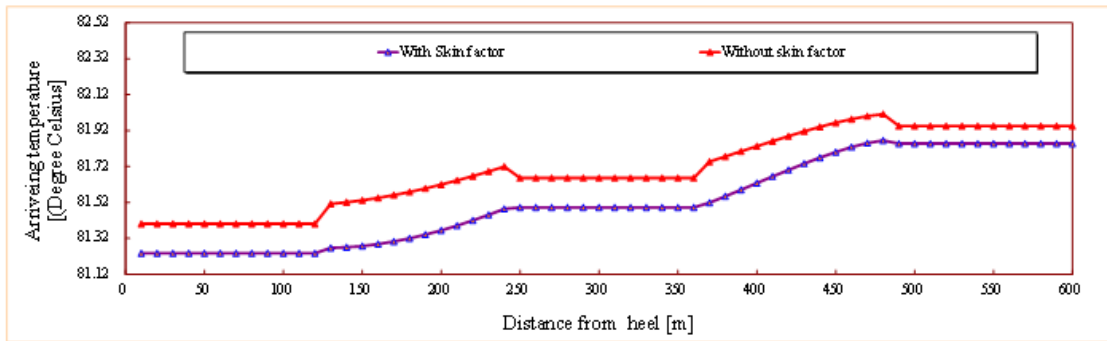


Figure 8. Arriving temperature profile with and without skin factor

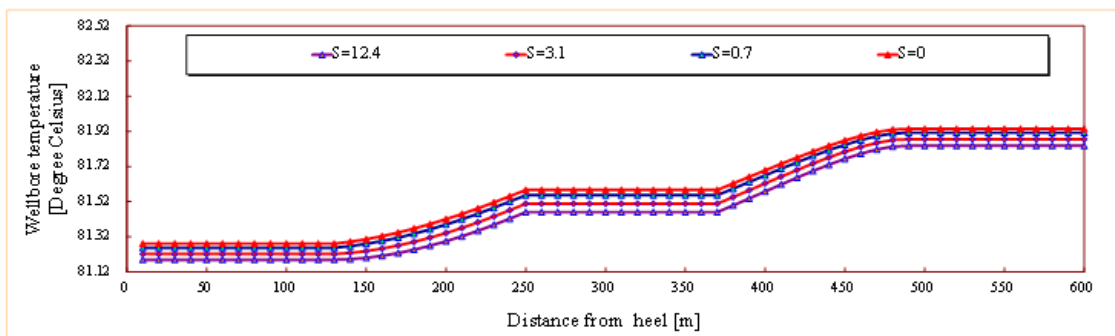


Figure 9. Wellbore temperature profile comparison between different skin factors

Figure 10 illustrates comparison between skin factors on the wellbore temperature derivative curve. When compared with the wellbore temperature profile (Fig. 9), the temperature derivative data from

non-perforated sections are almost constant, which phenomenon is helpful in identification of non-perforated wellbore sections.

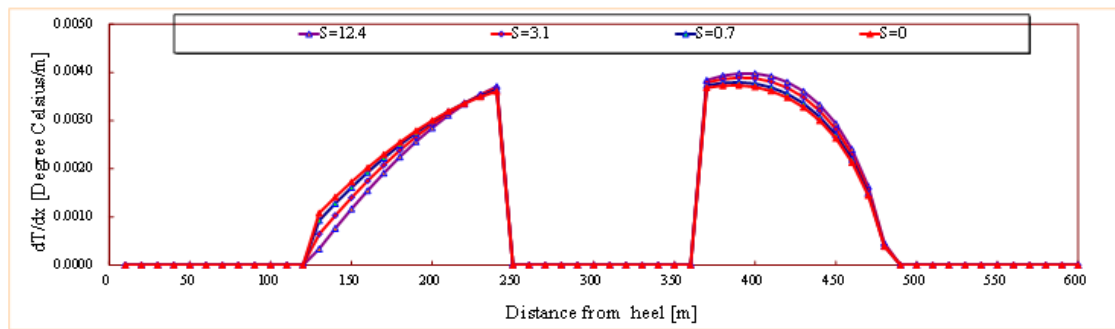


Figure 10. Temperature derivative comparison between different skin factors

Differences between arriving temperature and wellbore temperature are shown in Figure 11, where the non-perforated sections are also easily recognized by a horizontal line. In addition, the temperature difference is smaller here, accounting for greater skin factor due to intensified Joule-Thomson effect near the wellbore.

As mentioned earlier, the temperature along wellbore is also related to non-Darcy flow factor. First, the arriving temperature profile is to be ana-

lyzed, whose profile comparison with and without non-Darcy flow factor is depicted in Figure 12. As shown, the arriving temperature with non-Darcy flow factor is less than that without non-Darcy flow factor, the reason for which is generation of greater pressure loss near the wellbore under non-Darcy flow phenomenon, in turn producing decreased arriving temperature by the Joule-Thomson effect. In addition, perforated sections may also be easily recognized by jumping data.

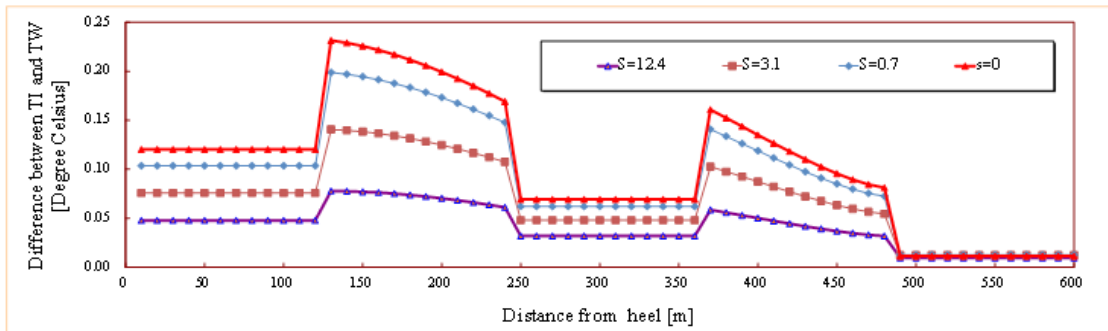


Figure 11. Difference between arriving temperature and wellbore temperature

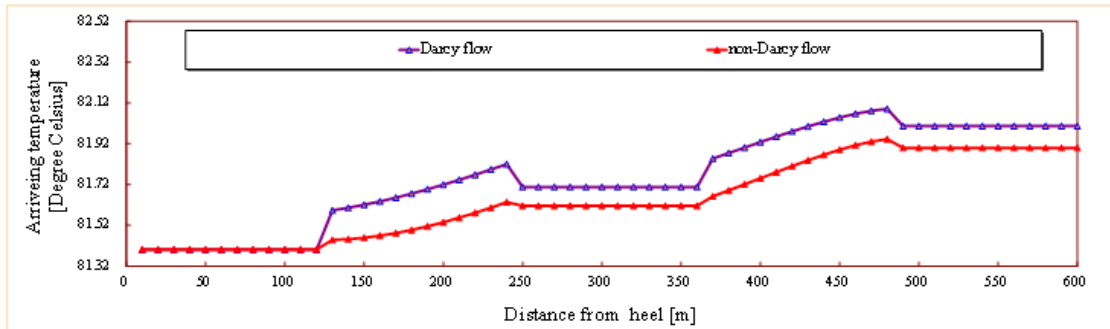


Figure 12. T_i with and without non-Darcy flow factor

Figure 13 illustrates the wellbore temperature profile comparison between different non-Darcy flow factors, and Figure 14 shows temperature differences between the arrival location and the wellbore. Both figures display perforated sections and non-perforated sections, however Figure 14 is more clear. As well, the non-Darcy flow factor affects the wellbore temperature. According to Figure 13, greater non-Darcy

flow factor generates lesser wellbore temperature due to reduced arriving temperature. Furthermore, Figure 14 confirms that greater non-Darcy flow factor generates increased temperature differential between arrival location and the wellbore along perforated sections. Temperature differential is minimal along non-perforated sections, providing a basis for non-perforated sections judgment.

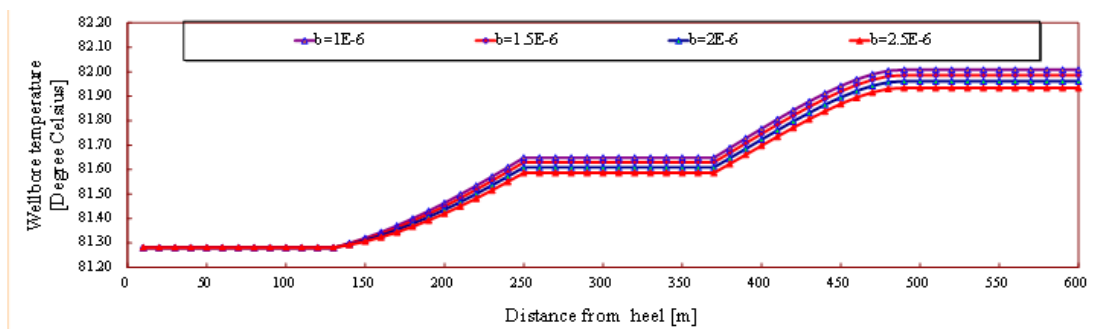


Figure 13. Wellbore temperature profile comparison of different non-Darcy flow factors

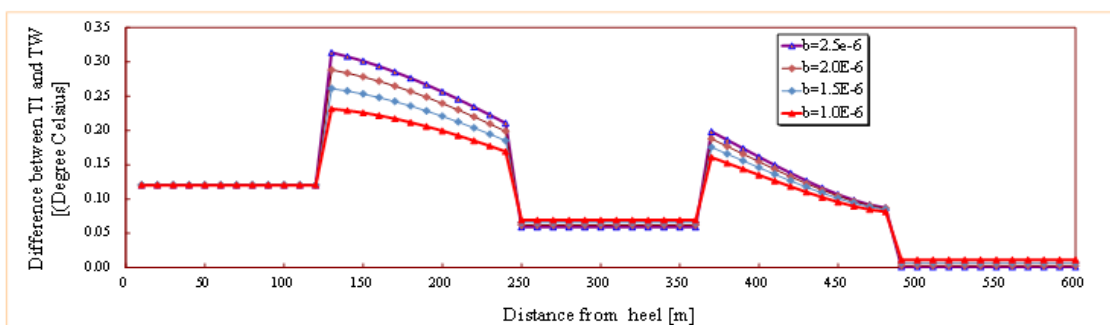


Figure 14. Difference between arriving temperature and wellbore temperature

Temperature along the wellbore is also related to well completion methods, for which consideration Figure 15 presents 4 different well completion methods with constant wellbore length. It is assumed that the horizontal well is producing at a constant pro-

duction rate of $60000\text{m}^3/\text{d}$, without consideration of skin factor and non-Darcy flow, but considering the Joule-Thomson effect. By calculating 4 cases, temperature and temperature derivative curves (Fig.16) were derived and plotted.

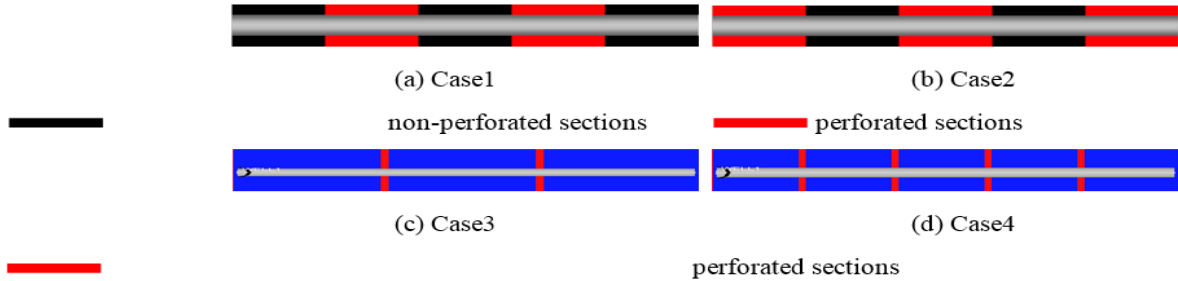


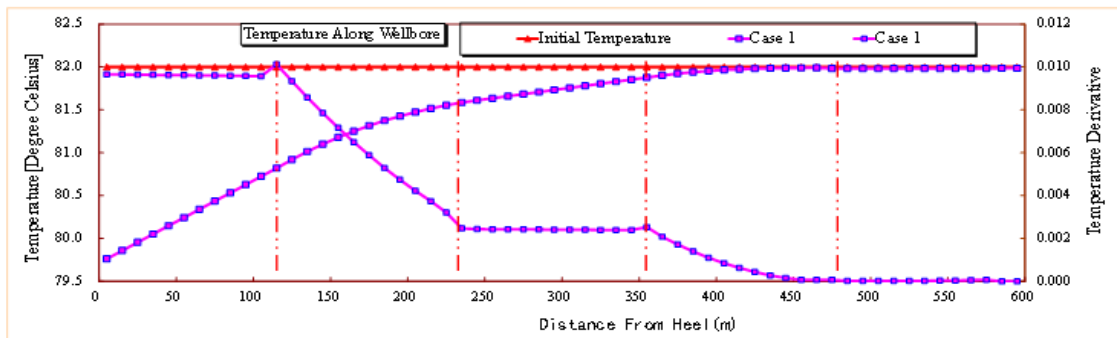
Figure 15. Schematic Diagrams of 4 Well Completion Methods

It can be seen from Figure 16 a-d that well completion methods have a significant effect on temperature distribution and temperature derivative, especially along the perforated areas. However, according to the temperature derivative curves, the impacts are relatively moderate along the non-perforated interval.

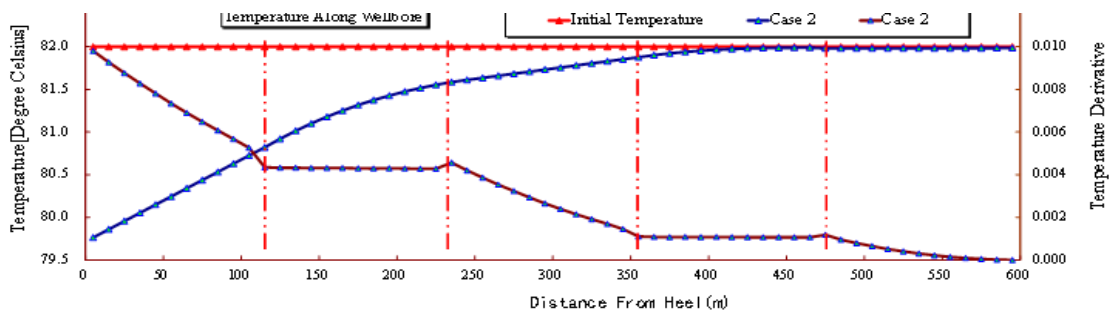
Figures 16(a) and (b) present temperature derivative curves for non-perforated sections as horizontal lines, while the perforated sections vary. The difference here is caused by lack of gas flow into the wellbore along non-perforated sections. As a result, wellbore temperature decrease is constant due to con-

stant gas flow rate in the wellbore. By contrast, gas continuously flows into the wellbore along the perforated sections, thus gradually increasing the gas flow velocity in the wellbore, leading to a greater temperature decrease.

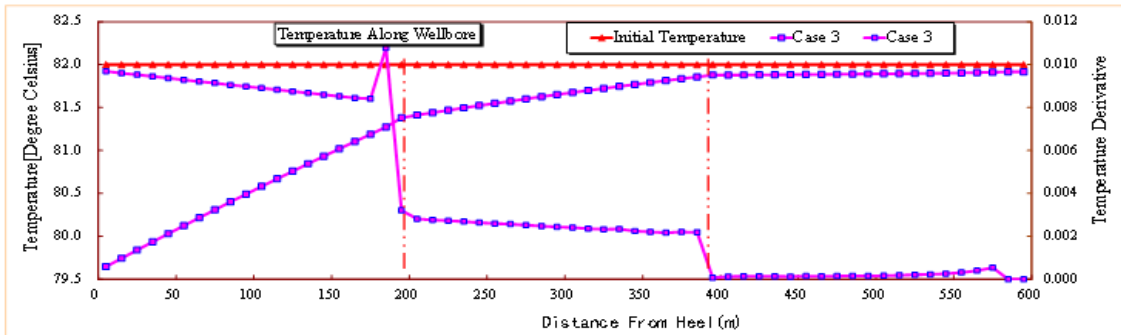
The influences of manufactured fractures on temperature and temperature curve can be seen in Figures 16 c and d, where temperature curves decrease significantly along the fractured sections. In the same position, however, temperature derivative curves for the fractured sections show data jumps, easing identification of fractures.



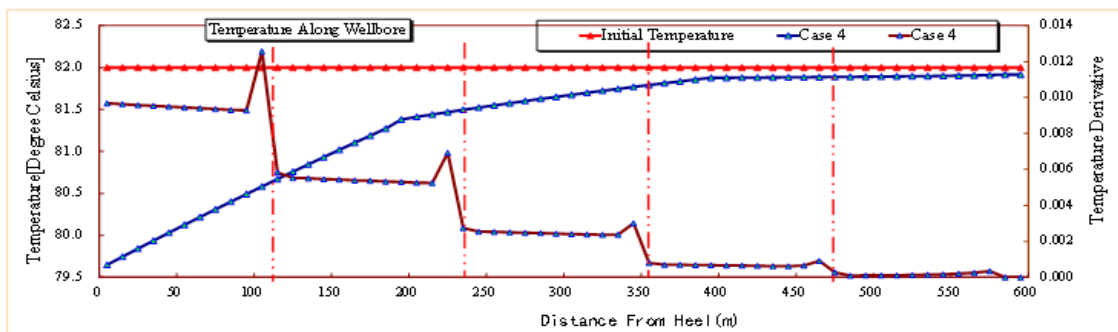
(a)



(b)



(c)



(d)

Figure 16. Effect of Well Completion Method on Temperature and Derivative

5. Conclusions And Recommendations

A wellbore temperature model for hydraulic-fracturing horizontal wells in gas reservoirs is established in this paper, which considers skin factor and non-Darcy flow factor. This model can be applied to predict the temperature along the wellbore. By studying both coupled reservoir and wellbore temperature models, temperature response type curves may be plotted by algorithm, and temperature influence factors may also be analyzed.

Here, skin factor, non-Darcy flow factor and well completion method are all demonstrated to affect temperature along the wellbore. As well, variations in data may serve as indicator for identification of perforated sections.

This progressive model is the basis of interpreting temperature phenomena in hydraulic-fracturing horizontal wells. On this basis, future investigation should produce a needed inverse model, able to translate DTS data into flow rate profile, skin factor and other physical characteristics, further refining drilling and extraction processes.

References

1. Hill, A.D. (1990) Production Logging-Theoretical and Interpretive Elements, *Society of Petroleum Engineers Inc.* Richardson, TX.
2. Brown, G., Storer, D., McAllister, K., Al-Asi

mi, M., and Raghavan, K. (2003) Monitoring-Horizontal Producers and Injectors During Cleanup and Production Using Fiber-Optic-Distributed Temperature Measurements, *paper SPE 84379 presented at the SPE Annual Technical Conference and Exhibition*, Denver, CO.

3. Tolan, M., Boyle, M., and Williams, G. (2001) The Use of Fiber-Optic Distributed Temperature Sensing and Remote Hydraulically Operated Interval Control Valves for the Management of Water Production in the Douglas Field, *paper SPE 71676 presented at the 2001 SPE Annual Technical Conference and Exhibition*, New Orleans, LA.
4. Foucault, H., Poilleux, D., Djuricic, A., Slikas, M., Strand, J., and Silva, R. (2004) A Successful Experience for Fiber Optic and Water Shut Off on Horizontal Wells with Slotted Liner Completion in an Extra Heavy Oil Field, *paper SPE 89405 presented at the 2004 SPE/DOE Fourteenth Symposium on Improved Oil Recovery*, Tulsa, OK.
5. Fryer, V., ShuXing, D., Otsubo, Y., Brown, G. and Guilfoyle, P. (2005) Monitoring of Real-Time Temperature Profiles Across Multi-zone Reservoirs during Production and Shut

- in Periods Using Permanent Fiber-Optic Distributed Temperature Systems. *Paper SPE presented at SPE Asia Pacific Oil and Gas Conference and Exhibition*, Jakarta, Indonesia.
6. Johnson, D., Sierra, J., Kaura, J. and Gualtieri, D. (2006) Successful Flow Profiling of Gas Wells Using Distributed Temperature Sensing Data. *Paper SPE 103097 presented at SPE Annual Technical Conference and Exhibition*, San Antonio, Texas, USA.
 7. Huebsch H T, Moss M, Trilsbeck T C, et al. (2008) Monitoring Inflow Distribution in Multizone Velocity String Gas Wells Using Slickline Deployed Fiber Optic Distributed Temperature Measurements[C]. *SPE Annual Technical Conference and Exhibition*. Society of Petroleum Engineers.
 8. Julian, J. Y., King, G. E., Cismoski, D. A., Younger, R. O., Brown, D. L., Brown, G. A., Richards, K. M., Meyer, C. A., Sierra, J. R., Leckband, W. T., Sack, J. K. and Julian, F. C. (2007) Downhole Leak Determination Using Fiber-Optic Distributed-Temperature Surveys at Prudhoe Bay, Alaska. *Paper SPE 107070 presented at SPE Annual Technical Conference and Exhibition*, Anaheim, California.
 9. Huckabee, P. (2009) Optic Fiber Distributed Temperature for Fracture Stimulation Diagnostics and Well Performance Evaluation. *Paper SPE presented at SPE Hydraulic Fracturing Technology Conference*, The Woodlands, Texas.
 10. Li Z. (2010) Interpreting Horizontal Well Flow Profiles and Optimizing Well Performance by Downhole Temperature and Pressure Data. *Texas A&M University*.
 11. Gonzalez L E, Chokshi R. (2012) Wellbore Real-Time Monitoring and Analysis for Shale Reservoirs. *SPE Americas Unconventional Resources Conference*. Society of Petroleum Engineers.
 12. Ramey Jr H J. (1962) Wellbore heat transmission. *Journal of Petroleum Technology*, 14(04), p.p.427-435.
 13. Satter A. (1965) Heat losses during flow of steam down a wellbore. *Journal of Petroleum Technology*, 17(7), p.p.845-851.
 14. Witterholt E J, Tixier M R. (1972) Temperature logging in injection wells[C]. *Fall Meeting of the Society of Petroleum Engineers of AIME*. Society of Petroleum Engineers.
 15. Steffensen R J, Smith R C. (1973) The Importance of Joule-Thomson Heating (or Cooling) in Temperature Log Interpretation. *Fall Meeting of the Society of Petroleum Engineers of AIME*. Society of Petroleum Engineers.
 16. Miller C W. (1979) Wellbore storage effects in geothermal wells. *California Univ., Berkeley (USA)*. Lawrence Berkeley Lab.
 17. Sagar R, Doty D R, Schmidt Z. (1991) Predicting temperature profiles in a flowing well. *SPE production engineering*, 6(4), p.p. 441-448.
 18. Hasan A R, Kabir C S. (1994) Aspects of wellbore heat transfer during two-phase flow (includes associated papers 30226 and 30970). *SPE Production & Facilities*, 9(3), p.p.211-216.
 19. Izgec B. (2008) Transient fluid and heat flow modeling in coupled wellbore/reservoir systems. *Texas A&M University*.
 20. Yoshioka, K. (2007) Detection of Water or Gas Entry into Horizontal Wells by Using Permanent Downhole Monitoring System. *PhD thesis, Texas A&M University*, College Station, Texas.
 21. Zhuoyi Li, Ding Zhu (2010) Predicting. Flow Profile of Horizontal Well by Downhole Pressure and Distributed-Temperature Data for Waterdrive Reservoir. *SPE Production & Operations*, 08.
 22. Yoshioka K, Zhu D, Hill A D, et al. (2005) Interpretation of Temperature and Pressure Profiles Measured in Multilateral Wells Equipped with Intelligent Completions (SPE94097). *67th EAGE Conference & Exhibition*.
 23. Ouyang, L.-B., Arbabi, S. and Aziz, K. (1998) General Wellbore Flow Model for Horizontal, Vertical, and Slanted Well Completions. *SPE Journal*, 3(2), p.p.124-133.
 24. Willhite, G. P. (1967) Over-all Heat Transfer Coefficients in Steam And Hot Water Injection Wells. *Journal of Petroleum Technology* 19 (5), p.p.607-615.